



OPEN

SUBJECT AREAS:

BIOCHEMISTRY

BIOTECHNOLOGY

BIOMATERIALS - PROTEINS

Received
6 August 2014Accepted
19 November 2014Published
9 December 2014Correspondence and
requests for materials
should be addressed to
L.X. (linxu@jlu.edu.cn)
or H.S. (songhw@jlu.
edu.cn)

Ultrasensitive non-enzymatic glucose sensor based on three-dimensional network of ZnO-CuO hierarchical nanocomposites by electrospinning

Chunyang Zhou, Lin Xu, Jian Song, Ruiqing Xing, Sai Xu, Dali Liu & Hongwei Song

State Key Laboratory on Integrated Optoelectronics, College of Electronic Science and Engineering, Jilin University, 2699 Qianjin Street, Changchun, 130012, People's Republic of China.

Three-dimensional (3D) porous ZnO-CuO hierarchical nanocomposites (HNCs) nonenzymatic glucose electrodes with different thicknesses were fabricated by coelectrospinning and compared with 3D mixed ZnO/CuO nanowires (NWs) and pure CuO NWs electrodes. The structural characterization revealed that the ZnO-CuO HNCs were composed of the ZnO and CuO mixed NWs trunk (~200 nm), whose outer surface was attached with small CuO nanoparticles (NPs). Moreover, a good synergetic effect between CuO and ZnO was confirmed. The nonenzymatic biosensing properties of as prepared 3D porous electrodes based on fluorine doped tin oxide (FTO) were studied and the results indicated that the sensing properties of 3D porous ZnO-CuO HNCs electrodes were significantly improved and depended strongly on the thickness of the HNCs. At an applied potential of + 0.7 V, the optimum ZnO-CuO HNCs electrode presented a high sensitivity of 3066.4 $\mu\text{AmM}^{-1}\text{cm}^{-2}$, the linear range up to 1.6 mM, and low practical detection limit of 0.21 μM . It also showed outstanding long term stability, good reproducibility, excellent selectivity and accurate measurement in real serum sample. The formation of special hierarchical heterojunction and the well-constructed 3D structure were the main reasons for the enhanced nonenzymatic biosensing behavior.

Enzymeless amperometric glucose sensors have attracted extensive attention for its high repeatability and stability compared to enzymatic sensors, which have practical significance in both clinical diagnosis and food industries¹⁻⁵. However, since most enzymeless glucose sensors rely on the chemical activity of transition metal centre which can be easily poisoned, fabrication of the enzymeless glucose sensing elements with high performance remains a challenge. Generally, an efficient glucose sensor should be reasonably evaluated by many parameters according to need, such as high sensitivity, fast response, good selectivity and stability, the pH environment, and working voltage. Thus, a good enzymeless sensor which can meet those conditions and come to the fore should be associated not only with the composition and surface properties of the sensing materials, but also with their microstructures.

As a p-type semiconductor with high chemical activity and nontoxic nature, CuO has been a widely investigated material for using as an enzymeless glucose biosensor due to its outstanding redox behavior⁶⁻⁹. With advance of the related research, 1D CuO based hierarchically nanostructure are considered to be promising enzymeless amperometric candidate to effectively detect glucose with higher selectivity and sensitivity¹⁰⁻¹¹, because of their high surface to volume ratios and special physicochemical properties. Besides, thanks to the strong interactions between the closely packed nanounits, sensing characteristics can be further enhanced or tuned by appropriate combining two kinds of semiconductor oxides in CuO based hierarchical nanostructure. For example, in the mixed Ni-CuO-oxide NWs array, the corresponding sensitivity to glucose was proved to be as high as ~ 1600 $\mu\text{AmM}^{-1}\text{cm}^{-2}$ ¹². In addition, our recent work also revealed that the highly enhanced glucose sensitivity (1321 $\mu\text{AmM}^{-1}\text{cm}^{-2}$) could be obtained in CuO/TiO₂ based 1D hierarchical structures¹³. As is well known, ZnO is also a hot functional material in glucose sensing area, which possesses nice biocompatibility and fast electron transfer ability between the active sites and the electrode¹⁴⁻¹⁸. Moreover, the ZnO-CuO heterostructure has been expected to obtain enhanced performance and expands the potential applications of the heterogeneous nanodevices¹⁹⁻²². Xu et al. synthesized CuO-ZnO nanoporous gas sensor by transferring a solution-dipped self-organized colloidal template on to a device substrate, which exhibited shorter recovery time and



better selectivity to H₂S gas against other interfering gases²¹. Xia et al *in situ* prepared cluster-like nano/micro CuO/ZnO particles in dielectric barrier discharge for sensitive cataluminescence sensing of acetic acid²². However, synthetic approaches to 1D hierarchically ZnO–CuO nanostructures, which combine a high surface-to-volume ratio and an intimate interfacial contact of the components, remain in demand in sensing area.

On the other hand, from the view of the glucose sensor, the sensing process of enzymeless sensors based on semiconductor oxides generally involves a surface redox reaction. However, since most of the nanostructured electrodes are fabricated by printing the nano-object slurry onto a conductive substrate (such as drop or spin coating after dispersion), dense films will form and then lead to inhomogeneous thickness, poor reproducibility, and structural instability of the as fabricated electrodes. Consequently, the overall performance of the electrodes will be discounted. Due to such limited, efforts have been made to improve or modify the traditional film into integrated 3D porous network on purpose of obtaining the larger effective surface area, which are of great benefit for molecule diffusion and mass transport in sensor materials^{23–26}. Despite all this, as far as we know, little attention has been given to study the 3D electrode built with ZnO–CuO HNCs network and exploration of their enzymeless glucose sensing properties comprehensively.

In spire by this, we first designed an integrated 3D network built with 1D ZnO–CuO HNCs and carefully studied their enhanced enzymeless sensing properties for high sensitive detecting of glucose. At the same time, we also fabricated pure CuO NWs and mixed ZnO/CuO NWs by electrospinning for comparison. In ZnO–CuO HNCs, mixed ZnO/CuO NWs are the main stem, which provide a larger active surface area and plus a good electron transport path. Besides, some CuO NPs are surface attached on the main stem, which act as the specific and additional active sites for glucose sensing. It should be highlighted that, such a complex 3D structure can be easily obtained through one-step coelectrospinning together with ordinary hot press and calcination process. Moreover, the enzymeless sensing behaviors of the 3D ZnO–CuO HNCs electrodes with different thickness of 3D network toward glucose were investigated. Remarkable improvement of enzymeless sensing properties was observed.

Results and discussion

Morphologies and Structural Properties. The phase characteristics of ZnO–CuO HNCs as well as mixed ZnO/CuO NWs, pure CuO and ZnO NWs were first identified from the X-ray diffraction (XRD) patterns as presented in Fig. 1. The diffraction peaks of the mixed ZnO/CuO NWs and ZnO–CuO HNCs samples are perfectly indexed to the mixture of monoclinic CuO (JCPDS 48-1548) and hexagonal ZnO (JCPDS 36-1451). Besides, the relative intensity of the dominant diffraction peak of CuO is higher than that of ZnO in

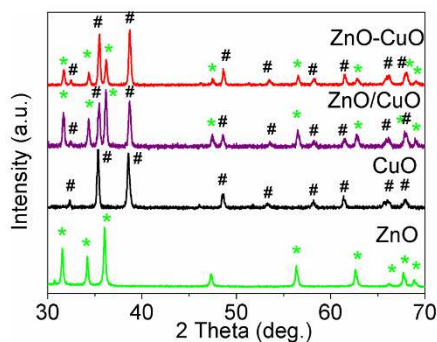


Figure 1 | The XRD of 3D ZnO–CuO HNCs, mixed ZnO/CuO NWs, pure CuO and ZnO NWs samples. The XRD peaks of CuO (JCPDS no.48-1548) are marked with “#” and ZnO (JCPDS no.36-1451) are marked with “*”.

ZnO–CuO HNCs, suggesting the better crystallinity of CuO in hierarchical sample. However, the situation of crystalline in mixed ZnO/CuO NWs is in the opposite way, which indicated a different arrangement of ZnO and CuO grains in these two samples.

Fig. 2a and 2b show the scanning electron microscopy (SEM) images of the as-fabricated 3D porous ZnO–CuO HNCs. These randomly oriented HNCs all have uniform and long continuous surface in a large scale. In each HNCs structure there are some small NPs (~20 nm in diameter) attached randomly on the surface of the NWs, whose outer diameters are ~200 nm. Fig. 2c and 2d are the low- and high-magnification cross section SEM images of the 3D ZnO–CuO HNCs electrode (20 min). As is observed that the uniform 3D film is formed with thickness of $13.5 \pm 0.3 \mu\text{m}$ and the hierarchical structure remains after hot pressing. Besides, the porous structure in the thickness dimension can be clearly identified, which is an obvious evidence of the effective formation of 3D porous electrode. Note that all the 3D porous ZnO–CuO HNCs electrodes have the similar planar morphology, but with different thicknesses as shown in Fig. S1a–f. In detail, the corresponding thicknesses are $5.3 \pm 0.3 \mu\text{m}$ for 10 min, $7.8 \pm 0.4 \mu\text{m}$ for 15 min, and $18.0 \pm 0.5 \mu\text{m}$ for 25 min coelectrospinning time. Fig. 2e and Fig. 2f shows the planar morphology of 3D pure CuO NWs and 3D mixed ZnO/CuO NWs electrodes for compare, the average diameter are both ~200 nm and the thickness of corresponding 3D electrodes (not shown) are also comparable with that of the 3D ZnO–CuO HNCs electrode (20 min). The morphology of 3D pure ZnO NWs are also provided for comparing as shown in Fig. S1g and h, which exhibits much smoother surface than the other samples, thus the thickness of corresponding 3D electrodes (20 min) is relatively thick ($11.1 \pm 0.5 \mu\text{m}$).

The heteroarchitecture of the ZnO–CuO HNCs can be further confirmed from transmission electron microscopy (TEM) image (Fig. 3a). The as marked interplanar distances of the fringes are 0.232 nm and 0.252 nm, corresponding to the (111) face of CuO and the (101) face of ZnO, respectively (Fig. 3b). Further, as shown in energy dispersive X-ray (EDX) mappings (Fig. 3c–e), the

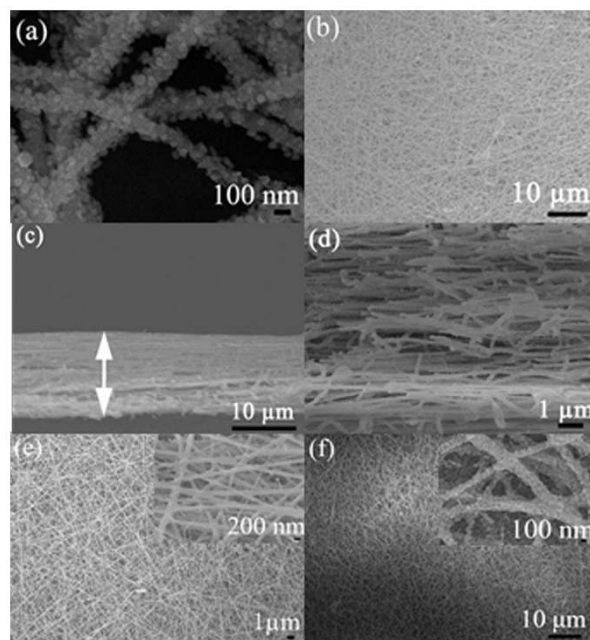


Figure 2 | (a) and (b) typical SEM image of 3D porous ZnO–CuO HNCs electrode (20 min) on the surface of FTO. (c) and (d) the low- and high-magnification cross section SEM images of (b). (e) The SEM image of 3D pure CuO NWs electrode. The inset of (e) is its high-magnification SEM image. (f) The SEM image of 3D mixed ZnO/CuO NWs and its inset is high-magnification SEM image.

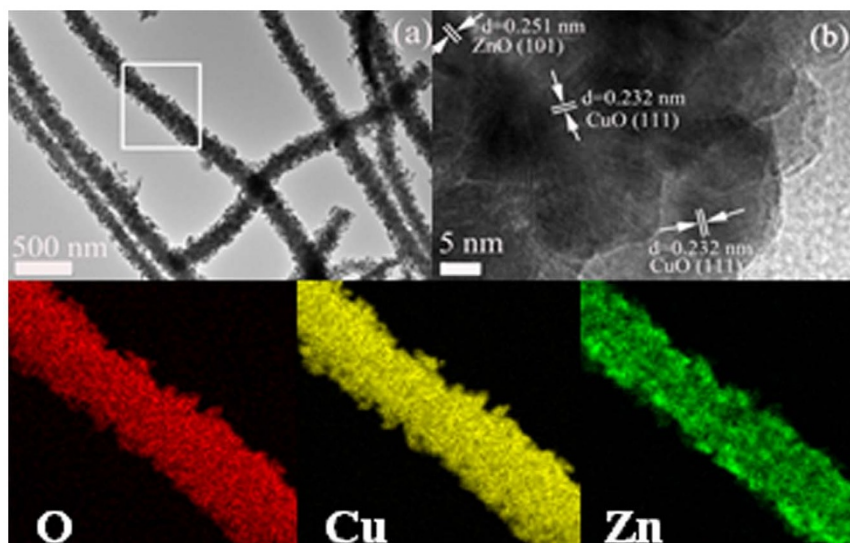


Figure 3 | (a) TEM image and (b) HR-TEM image of ZnO–CuO HNCs. (c), (d), and (e), EDX elemental mapping images of O, Cu, and Zn in the ZnO–CuO HNCs sample taken from the box of (a).

distribution of Cu element is similar with that of O, which shows a hierarchical structure with uniform and discontinuous NPs on the surface of NWs trunk. The distribution of Zn element is much more homogeneous, which only shows a NWs structure. This demonstrates that the NWs trunk is composed of uniform mixture of CuO and ZnO, and the NPs dispersed on the outer surface of the NWs trunk are mainly composed of CuO.

To reveal the surface composition and chemical state of the elements existing in the ZnO–CuO HNCs sample, X-ray photoelectron spectroscopy (XPS) spectra were studied and compared with that of the mixed ZnO/CuO, pure CuO NWs and ZnO NWs as shown in Fig. 4. First, the complete spectra of the samples confirm the presence of Cu, O, and C atoms in pure CuO NWs, Zn, O, and C atoms in pure ZnO NWs and Cu, Zn, O, and C atoms in ZnO–CuO HNCs and mixed ZnO/CuO NWs. Moreover, based on XPS spectra, the atom ratios of Cu/Zn have been quantitatively calculated to be 0.34 and 0.72 corresponding to the mixed ZnO/CuO and ZnO–CuO HNCs samples, respectively. As can be seen, the combination rate is relatively low for CuO in mixed ZnO/CuO, even the initial molar ratio of Zn/Cu is about 0.82. However, although the initial quantity is the same both in the mixed ZnO/CuO and ZnO–CuO HNCs samples, the atom ratio of Cu/Zn is 2.1 times higher in ZnO–CuO HNCs sample than that in mixed ZnO/CuO, this can be attributed to the formation of the special HNCs structure which has CuO NPs decorated on the surface of mixed ZnO/CuO NWs, and thus the atom ratio of Cu/Zn increases.

The corresponding O 1s XPS spectra are enlarged in Fig. 4b. Accordingly, the O1s XPS spectra of ZnO–CuO HNCs and mixed ZnO/CuO NWs samples display four peaks. The binding energies around 530.7 eV and 532 eV correspond to the lattice oxygen in crystalline CuO and ZnO, respectively. Compared to the pure CuO and ZnO NWs, the binding energies of CuO in ZnO–CuO HNCs and mixed ZnO/CuO NWs samples both shift, indicating a modification of the electron density on CuO due to the interactive coupling between CuO and ZnO²⁷, and because of the different nanostructure in ZnO–CuO HNCs and mixed ZnO/CuO NWs samples, the shift direction shows somewhat different. The O 1s peaks around 532.9 eV is assigned to the deficient oxygen and the peak around 533.7 eV in all the three samples belongs to the chemisorbed or dissociated oxygen or OH species on the samples.

The high resolution XPS spectra of Cu 2p are shown in Fig. 4c. The peaks around 934.4 eV and 954.4 eV in all the three samples confirm the presence of Cu 2p_{3/2} and Cu 2p_{1/2} peaks, respectively²⁷. Along

with the main peak around 934.4 eV, the shake-up satellite peaks are observed at the higher binding energy side, 943.1 and 963.0 eV, which are characteristics of partially filled d-block (3d₉) of Cu²⁺²⁸. The peak locations and relative intensities of the satellites against the core levels are indicative of the formation of CuO. In addition, the location of the Cu 2p XPS peaks in mixed ZnO/CuO NWs samples shifts to lower binding energy compared to pure CuO NWs²⁸. This clearly indicates a modification of the electron density on CuO species due to the interactive coupling between CuO and ZnO and leading the increased surface activity of CuO. In ZnO–CuO HNCs sample, after surface decorating of CuO NPs on mixed ZnO/CuO NWs, the Cu 2p XPS peaks shifts to higher binding energy and comparable with that of pure CuO NWs, indicating the nanostructure of surface decorated CuO NPs were well maintained after the formation of the hybrid ZnO–CuO HNCs structure, which have been observed and proved in some similar structures^{29–30}.

The detailed XPS chemical environment of Zn 2p in mixed ZnO/CuO NWs, ZnO–CuO HNCs and ZnO NWs are shown in Fig. 4d. The Zn 2p spectra both show two symmetric peaks, the peak around 1022.5 eV corresponds to the Zn 2p_{3/2} and the one around 1045.5 eV is assigned to Zn 2p_{1/2}, indicating a normal state of Zn 2p in the samples³¹. Compared to pure ZnO NWs, the Zn 2p core level region of ZnO–CuO HNCs and mixed ZnO/CuO NWs samples shift to the higher binding energy after introduction of CuO, but with the same splitting between Zn 2p_{1/2} and Zn 2p_{3/2} (~23 eV). The shift of Zn 2p peaks to higher binding energy can be explained by the strong interaction between ZnO and CuO nanocrystals in the two samples. In ZnO–CuO HNCs sample, the same with the Cu 2p XPS spectra, the Zn 2p XPS peaks also shift to higher binding energy compared with that of mixed ZnO/CuO NWs, further indicating local environment of ZnO and CuO NPs are different in ZnO–CuO HNCs and mixed ZnO/CuO NWs.

Nonenzymatic glucose behavior in different 3D porous electrodes.

The cyclic voltammetry profiles of 3D porous ZnO–CuO HNCs electrodes as well as 3D mixed ZnO/CuO NWs, pure CuO NWs and ZnO NWs electrodes in 30 mL 0.1 M NaOH solution without and with 5 mM glucose were studied (Fig. 5). The corresponding nonenzymatic response process to glucose is as depicted in Fig. 6. The Cu(II)/Cu(III) redox couple in the NaOH solution under the special potential region is the essential factor for nonenzymatic electrochemical glucose detection. When in blank NaOH solution, obvious reduction peaks around +0.7 V can be observed of all the

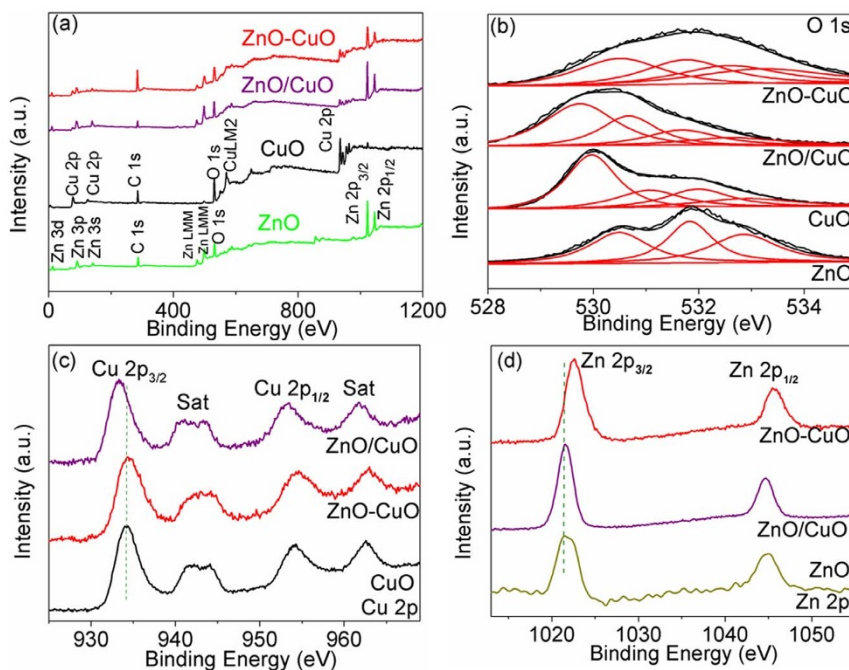
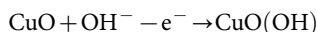


Figure 4 | (a) Survey, (b) O 1s, (c) Cu 2p, and (d) Zn 2p high resolution XPS spectrum of the corresponding samples.

electrodes (except pure ZnO NWs electrode) in our work which corresponding to the Cu(II)/Cu(III) redox couple according to previous studies³², the reaction process can be depicted as:



After the injection of glucose, Cu(III) ion obtains an electron and acts as an electron delivery system^{32–34}, electrons are transferred from glucose to the electrode which leads to the increasing of the peak current, the reaction process is as follows:



In addition, in Fig. 5a and Fig. 5b, the peak current intensity and current signal toward the positive end of the potential range drastically increases in 3D porous ZnO–CuO HNCs electrodes (20 min), which is ascribed to the increase of the electroactive surface area in ZnO–CuO HNCs¹⁸. Note that ZnO has no specific property of redox reaction like CuO, thus the pure ZnO NWs electrodes has no response to the glucose in enzymeless detection process as shown in Fig. 5a, and the role of ZnO in our nonenzymatic sensors is to

accelerate the electron transfer, as evidenced in Fig. 5 and Fig. S2 (EIS spectra).

Moreover, as can be seen in Fig. 5c, the peak current intensity increases gradually when the electrospun time changes from 10 min to 20 min and then decreases when electrospun time further increased to 25 min. That is to say, whatever comparing to 3D mixed ZnO/CuO NWs and pure CuO NWs electrodes with the same electrospun time (20 min) or the other 3D porous ZnO–CuO HNCs electrodes with different thickness, the 3D porous ZnO–CuO HNCs electrode (20 min) always exhibits the best electrochemistry behavior. This phenomenon indicates that a reasonable-built and well-structured 3D structure can effectively accelerate the electron transfer. In addition, The CV measurement of 3D porous ZnO–CuO HNCs (20 min) electrode was further performed in 0.1 M NaOH solution at different scan rates (Fig. 7). The peak current shows a linear response to the scan rate, implying a surface-controlled electrochemical process⁷.

Fig. 8a shows the I-t curve of different 3D electrodes performed at +0.7 V (vs. Ag/AgCl) in 0.1 M NaOH solution by addition of different concentration of glucose. It is clear that well-defined and fast amperometric responses are observed, except the pure ZnO NWs electrode which also has no response to glucose in I-t curve. The

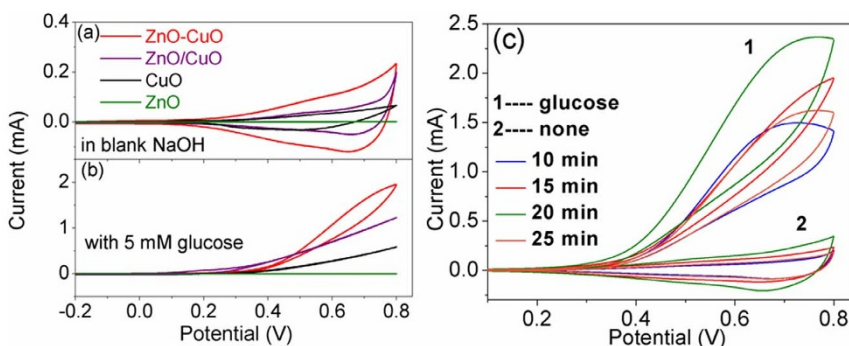


Figure 5 | The CV curves of 3D porous ZnO–CuO HNCs as well as mixed ZnO/CuO NWs, pure CuO and ZnO NWs electrodes both fabricated for 20 min in (a) blank NaOH solution and (b) NaOH solution with 5 mM glucose; (c) CV curves of 3D porous ZnO–CuO HNCs electrodes (10, 15, 20, 25 min) in 0.1 M NaOH in the absence (trace 2) and presence of 5 mM glucose (trace 1), respectively. The scan rate is 100 mV/s.

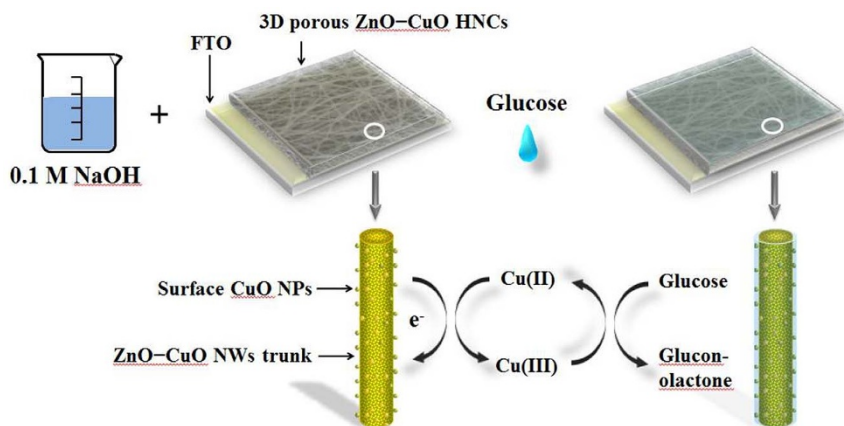


Figure 6 | Reaction mechanism of 3D porous ZnO–CuO HNCs electrodes. (the image of the flask are painting according to the model in our experiment by Lin Xu, one of the author of this article).

average times required approaching the steady-state current for the 3D pure CuO NWs electrode is 5 s, mixed ZnO/CuO NWs electrode is 3.4 s and 3D porous ZnO–CuO HNCs electrodes with electrospun time of 10, 15, 20, and 25 min were about 2.1, 1.6, 1.2, and 1.8 s, respectively, when the electrodes responded to 200 μM glucose. This indicates a rapid oxidative process in as-prepared 3D porous electrodes which is much faster than those in similar determination^{12,35}. Besides, the response times of the 3D porous electrodes modified by the samples which contain ZnO and CuO (mixed ZnO/CuO NWs and porous ZnO–CuO HNCs) are shorter than that of pure CuO NWs one and the corresponding responses are also higher, indicating that the interaction between ZnO and CuO in the composite structures are conducive to accelerate electron transport. Moreover, for the 3D porous ZnO–CuO HNCs electrodes, which has CuO NPs decorated on the surface of mixed ZnO/CuO NWs, they even show more faster response times and higher response, which further verify the advantage of ZnO–CuO HNCs structure. In our work, the I-t curves of the thinnest (10 min) and the thickest (25 min) 3D porous ZnO–CuO HNCs electrodes both show decreasing trend. This phenomenon reveals that the thickness of 3D structure has great influence on the performance of the electrodes. On the one hand, if the thickness is not thick enough it will lead to the electrode contain too little active ingredient content due to the lower combination rate of CuO as evidenced in XPS spectra and cause the suppression of I-t curve. On the other hand, if the thickness too thick it will result in too long electronic transmission path or the bad contact between FTO conducting substrate and upper 3D porous

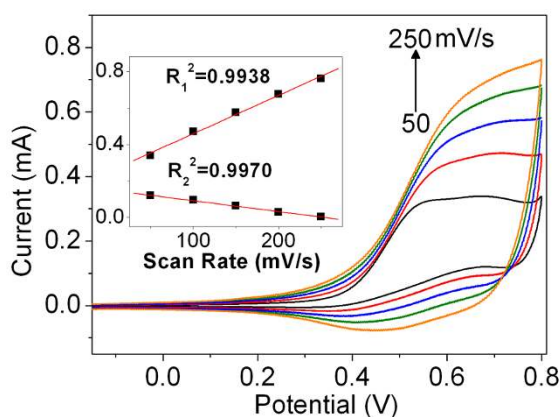


Figure 7 | CV curves of the 3D porous ZnO–CuO HNCs at various scan rates (50, 100, 150, 200, and 250 mV/s), inset is the plots of peak current vs. scan rate.

ZnO–CuO HNCs, then also cause the suppression of I-t curve. Note that a larger noise can be observed on the 3D porous ZnO–CuO HNCs electrode compared to the other contrastive electrodes in this study, this phenomenon can be ascribed to the formation of the hierarchical structure, which would increase the distance of each

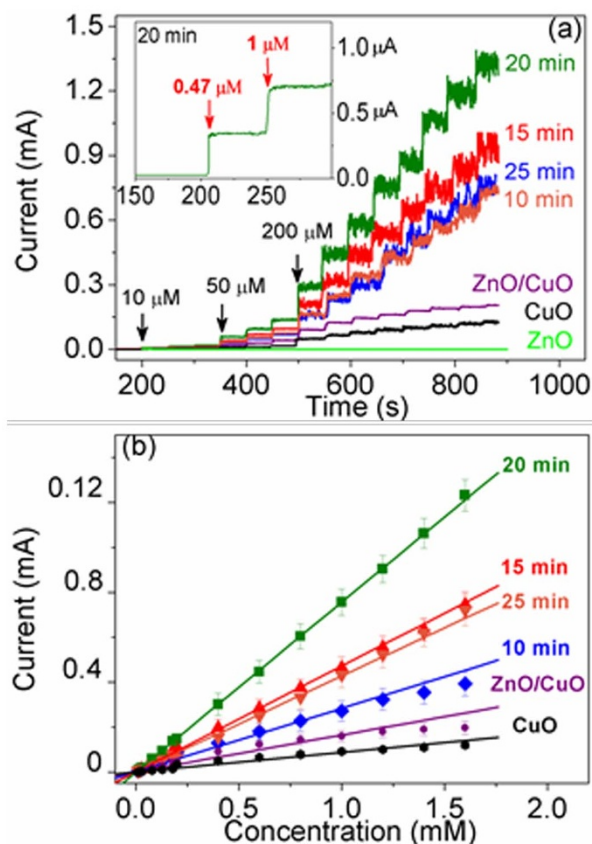


Figure 8 | (a) Amperometric response of 3D porous ZnO–CuO HNCs (10, 15, 20, and 25 min) electrodes as well as 3D mixed ZnO/CuO, 3D pure CuO and ZnO NWs electrodes at an applied potential of 0.7 V upon successive additions of different concentration of glucose in a step of 10, 50, and 200 μM , respectively for each current step, inset is the current response of 3D porous ZnO–CuO HNCs (20 min) to 0.47 and 1 μM glucose. (b) The corresponding calibration curve of current vs. concentration of glucose. The error bars denote the standard deviation of triplicate determination of each concentration of glucose.


Table 1 | A list of glucose sensing properties of different 3D electrodes in our study at an applied potential of 0.7 V

Electrodes	Sensitivity/ $\mu\text{AmM}^{-1}\text{cm}^{-2}$	R^2	Linear range	Detection limit/ μM
ZnO-CuO HNCs (10 min)	1680.2	0.9849	1.42 μM to 1.6 mM	0.52 μM
ZnO-CuO HNCs (15 min)	2080.7	0.9994	1.15 μM to 1.6 mM	0.78 μM
ZnO-CuO HNCs (20 min)	3066.4	0.9968	0.47 μM to 1.6 mM	0.21 μM
ZnO-CuO HNCs (15 min)	1876.5	0.9996	0.45 μM to 1.6 mM	0.38 μM
ZnO/CuO NWs	484	0.9654	2.5 μM to 1.6 mM	1.8 μM
CuO NWs	274.8	0.9846	4.6 μM to 1.6 mM	3.2 μM

HNCs in 3D network to some extent and further work should be carried out to avoid this effect.

The calibration curve of 3D electrodes is shown in Fig. 8b and the corresponding sensitivity, correlation coefficient, linear range, and detection limit under a signal/noise ratio of 3 are summarized in Table 1. As is compared, the 3D porous ZnO-CuO HNCs electrode (20 min) exhibits the best glucose biosensing performance in this work, which has the highest sensitivity of $3066.4 \mu\text{AmM}^{-1}\text{cm}^{-2}$, larger linear range from 0.47 μM to 1.6 mM, and the lower practical detection limit of 0.21 μM according to actual measurement data (as shown in inset of Fig. 8a). For the response time of the sensor for 0.47 μM glucose is calculated to be about 5.5, this is because low concentration of glucose need longer time to spread to the electrode-surface, which leads to the response time increased, compared with that to 200 μM glucose.

Further, we compared the performances of our best electrode with other published nonenzymatic glucose sensors based on CuO or electrospinning as listed in Table 2. It is clear that the sensitivity of our present electrode is largely improved and the integrative performance (sensitivity, detection limit and liner range) is also satisfactory. Although the detection limit of the 3D porous ZnO-CuO HNCs electrode (20 min) isn't the lowest one comparing to the electrodes as listed in Table 2, such as CuO SWCNTs and CuO NFs based electrodes^{9,37}, some particular advantages of the as prepared electrode in this work should be mentioned. First, from the view of practical application, the planar electrode based on FTO glass can easily integrate with the peripheral circuit and effectively reduce the volume of the circuit compared with the electrodes modified on the glassy carbon electrode. On the other hand, the upper film can be directly and steadily immobilized on the electrode through hot pressing, which could be used directly as the working electrode to detect glucose. Especially, hot pressing make the contact of the upper sensitive materials with electrode much closer and stable, thus compared to the CuO NFs modified on ITO, a larger linear range is obtained in the developed sensor³⁷. This method can greatly simplify the experimental steps. Based on the above analysis, we believe that the as prepared 3D porous ZnO-CuO HNCs electrodes have the potential ability to measure the glucose levels through saliva and other bodily

fluids which can obtain in a noninvasive way but possess much lower concentration glucose levels in the human body.

The enhanced non-enzymatic glucose performance of 3D porous ZnO-CuO HNCs electrode in our work can be ascribed it to the special hierarchical heterojunction formation in the composite and the well-constructed 3D porous structure. From the view of the special hierarchical heterojunction, as proved by Fig. 2, because of the particular hierarchical nanostructure which has suitable contacted area of n-type ZnO and p-type CuO (especially in NWs trunk), appropriate p-n junctions are formed and can create strong interaction, and this will be very favorable for the electron transmission (as proved by Fig. 4). Besides, the surface attached CuO NPs on NWs trunk can more effectively contact glucose, which will also helpful to improve the sensing performance (as proved by Fig. 4). In addition, from the point of the electrode structure, an integrated electron transport network is formed by the 3D porous framework. This network ensures the fast electron transport and suitable microcell environment for effective molecular diffusion. Moreover, since the 3D porous electrodes in our study work under surface-controlled electrochemical process, the effective surface area is critical, here, large surface area in the nanofibers and their 3D porous stacking mode can afford higher specific surface which provides large interface and unhindered diffusion of glucose molecules during kinetic mass transfer in the electrochemical process. It should be mentioned that such 3D electrode is controllable in microstructure (such as thickness) and of good reproducibility, and further, their high sensing performances to the target molecules could be controlled.

Reproducibility, selectivity, stability, and real sample detection.

To further verify the performance, some characteristics tests are performed on 3D porous ZnO-CuO HNCs electrodes. First, the intra-electrode and inter-electrode reproducibility of 3D porous ZnO-CuO HNCs electrode (20 min) for nonenzymatic glucose sensing were evaluated. Three modified electrodes were prepared, the relative standard deviations (RSD) is no more than 10.9% for the current response, indicating a satisfied electrode-to-electrode reproducibility. Additionally, the RSD of 6.7% ($n=3$) for 200 μM of glucose demonstrates good intra-electrode reproducibility.

Table 2 | A comparison of the sensing properties of 3D porous ZnO-CuO HNCs (20 min) with some other nonenzymatic glucose sensors based on CuO or electrospinning

Electrodes	Detection potential	Sensitivity $\mu\text{AmM}^{-1}\text{cm}^{-2}$	Linear range	Detection limit	Reference
ZnO-CuO HNCs	+0.7 V	3066.4	0.47 μM to 1.6 mM	210 nM	This work
CuO SWCNTs	+0.7 V	1610	0.05 μM to 1.8 mM	50 nM	[9]
CuO/TiO ₂	+0.7 V	1321	10 μM to 2 mM	390 nM	[13]
Cu _x O/PPy/Au	+0.6 V	232.22	6.2 μM to 8 mM	6200 nM	[35]
CuO NWs	+0.33 V	490	0.4 μM to 2 mM	49 nM	[36]
CuO NFs-ITO	+0.52 V	873	0.2mM to 1.3 Mm	40 nM	[37]
CuO NPs	+0.6 V	2762.5	0.05 mM to 18.4 mM	500 nM	[38]
CuO Pt/Ti/Si	+0.65 V	2900	1 μM to 2.5 mM	140 nM	[5]
CuO nanoparticles	+0.6 V	246	1 μM to 170 μM	910nM	[39]
CuO NSs	+0.5 V	2792.64	0.8 μM to 2.2 mM	800 nM	[40]

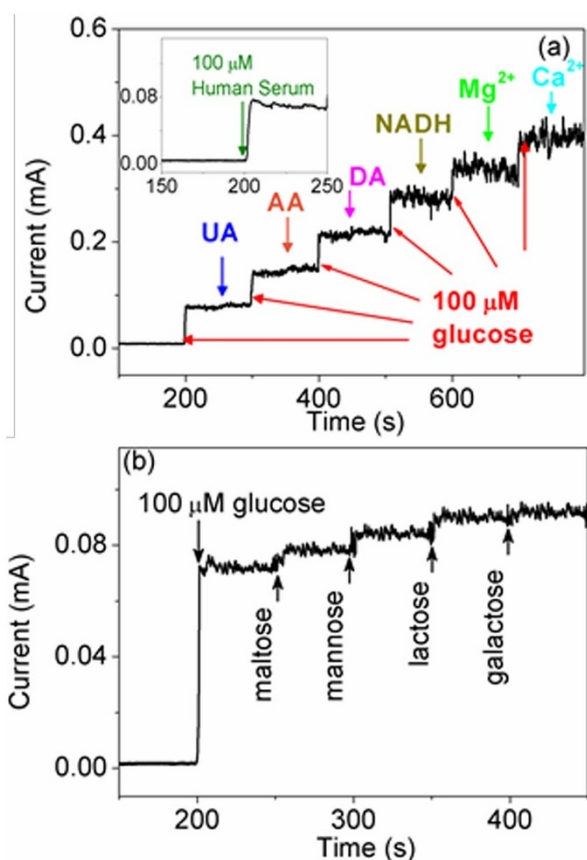


Figure 9 | The amperometric response of the 3D porous ZnO–CuO HNCs electrode (20 min) (a) with successive additions of different interfering species (UA, AA, DA, NADH, Mg^{2+} , and Ca^{2+}) and (b) with sequential addition of 10 μ M various interfering sugars (maltose, mannose, lactose, and galactose) after initial addition of 100 μ M glucose. The inset of (a) is its current response towards to 100 μ M glucose in human serum.

The electrochemical response of the interfering species of 3D porous ZnO–CuO HNCs electrode (20 min) was examined, as shown in Fig. 9. Although the concentration of interfering species in the human blood is 30 to 50 times less than that of glucose⁴¹, much higher concentrations of the interfering species (glucose : interfering species = 10 : 1) were used in the present analysis to ensure the sensitivity. First, some common interfering species in human serum, such as uric acid (UA), ascorbic acid (AA), dopamine acid (DA), nicotinamide adenine dinucleotide (NADH), Mg^{2+} , and Ca^{2+} , were chosen as the interfering species. As is clearly seen in Fig. 9a, the current responses of interfering species have little effect compared to glucose. In addition, other sugars, such as lactose, mannose, galactose, and maltose, are also present in abundant amounts in human blood, thus the selectivity to these organic compounds were also evaluated as shown in Fig. 9b. The current responses of the corresponding interfering species are also very low in the presence 100 μ M of glucose. Here, the

Table 3 | The glucose concentration in standardized human blood serum sample measured by the Accu-Chekabtive glucose meter and our 3D porous ZnO–CuO HNCs (20 min) electrode

	Glucose meter	Our sensor	RSD (%)
Reading	6.44 mM	6.76 mM	4.9%
Reading	6.44 mM	6.16 mM	4.3%
Reading	6.44 mM	6.92 mM	7.5%

good selectivity of 3D porous ZnO–CuO HNCs electrode (20 min) against to some reducing compounds, such as AA, can be ascribed to the obvious repulsion of negatively charged CuO and ZnO (the isoelectric point both are about 9.5) and the negatively charged AA (deprotonated) under highly basic conditions^{7,42,43}. The good selectivity of 3D porous ZnO–CuO HNCs electrode (20 min) for glucose and against other interfering materials can be ascribed to the synergistic action of well-designed 3D porous structure, high surface area and HNCs structure, which provide maximum numbers of active free paths to the glucose molecules and facilitate faster electron transfer (electronic kinetics).

Moreover, for real sample detection, the current response of 100 μ M glucose in human serum was also performed, as shown inset of Fig. 9b. An obvious current response can be observed after addition of 100 μ M human serum glucose. The concentration of glucose in the serum sample was calibrated using standard glucose solution and compared with the result obtained by the Accu-Chekabtive glucose meter (OLYMPUSAU 400). As presented in Table 3, the results from the biosensor are similar to those tested by the glucose meter, indicating the as-prepared biosensor may hold potential in real sample analysis. The long-term stability of the four different 3D porous ZnO–CuO HNCs electrodes (10, 15, 20, and 25 min) was also recorded which were tested once per week and the electrodes were stored in drying oven when not in use. As is calculated, the sensitivity decrease of four different 3D porous ZnO–CuO HNCs electrodes for the 10, 15, 20, and 25 min samples is 28.9%, 9.2%, 11.9%, and 6.9% within three weeks, respectively. This shows that the electrodes have a good stability and are favorable for their practical applications.

Conclusions

In conclusion, we have successfully in situ synthesized a series of 3D porous ZnO–CuO HNCs electrodes as well as 3D mixed ZnO/CuO, pure CuO and ZnO NWs electrodes as contrast experiments through a simple and controllable coelectrospinning and electrospinning procedure. The NWs trunk of ZnO–CuO HNCs was composed of uniform mixture of CuO and ZnO, and the NPs dispersed on the outer surface of the NWs trunk were mainly composed of CuO. In addition, it was confirmed that strong and different interaction existed between ZnO and CuO in 3D porous ZnO–CuO HNCs compared with that of in mixed ZnO/CuO, pure CuO and ZnO NWs, and then these samples were used to construct nonenzymatic glucose sensors. The optimal thickness of 3D porous ZnO–CuO HNCs electrodes is 13.5 μ m, corresponding to 20 min electrospinning time. It presents very high sensitivity of 3066.4 μ Amm⁻¹cm⁻², larger linear range up to 1.6 mM, and low practical detection limit of 0.21 μ M compared to the other electrodes and also shows strong stability, good reproducibility, excellent selectivity and accurate measurement in real serum sample. The reason can be attributed to special hierarchical heterojunction formation and the well-constructed 3D porous structure. Overall, on the basis of the electrochemical measurements, the 3D porous ZnO–CuO HNCs electrodes exhibit a great potential for use as a noninvasive nonenzymatic glucose biosensor.

Methods

Preparation of the samples. The ZnO–CuO HNCs were fabricated by one-step coelectrospinning followed by hot press and calcination. For the outer solution, 0.4 g of zinc acetate with two crystal water ($Zn(Ac)_2$) was dissolved in a mixed solvent composed of 4 mL N,N-dimethylformamide (DMF) and 1 mL ethanol at room temperature. After 15 min, 0.8 g of poly(vinyl pyrrolidone) (PVP, Mw = 130 000) was added and followed by vigorous stirring for 5 h to obtain the transparent outer sol solutions. In a similar way, 0.3 g of copper acetate with one crystal water ($Cu(Ac)_2$) was dissolved in the solution mixed by 2 mL DMF, 2 mL ethanol, and 2 mL acetic acid with magnetic stirring for 30 min at room temperature. Subsequently, 0.7 g PVP was added into the above mixture solution, followed by vigorous stirring for 12 h to obtain the final inner precursor solution.

The coelectrospinning setup used in this work has been described in detail in our previous literature⁴⁴. The collection distance between coaxial spinneret tip and collector was 15 cm, the applied steady-voltage was 15 kV, and the feeding rates of outer



and inner solution were 0.6 and 0.2 mL/h, respectively. The as-prepared precursor fibers were annealed with a rising rate of 1°C/min to 500°C and kept for 3 h, forming the ZnO–CuO HNCs. In addition, the mixed ZnO/CuO NWs and pure CuO NWs were prepared for comparison. For mixed ZnO/CuO NWs, the inner and outer solutions were mixed to obtain the precursor solution. For pure CuO and ZnO NWs, the inner and outer solution was used singly, respectively. Then, they were fabricated with the feeding rates of 0.6 mL/h and the other steps were the same with the preparation of ZnO–CuO HNCs. After the final calcination, the mixed ZnO/CuO NWs, pure CuO and ZnO NWs were obtained.

Preparation of the 3D porous electrodes. Before modification, FTO (1 × 2 cm, resistance ≤ 100 Ω) glasses were cleaned and dried. For the 3D porous ZnO–CuO HNCs electrodes, the FTO glass was put on the collector to collect fiber with the coelectrospinning time of 10, 15, 20, and 25 min, respectively. Then the as fabricated FTO electrodes were pressed for 1 min with the temperature of 140°C on the upper board and 80°C on the downward board and the thermocompressor was 1 kPa. Finally, the FTO electrodes were annealed at 500°C for 3 h with a rising rate of 1°C/min. In a similar way, the pure mixed ZnO/CuO, pure CuO and ZnO NWs modified electrodes were prepared for comparison, and the electrospinning time both were 20 min.

Characterization and Measurements. XRD patterns were conducted on Rigaku D/max 2550 X-ray diffractometer, using a monochromatized Cu target radiation resource ($\lambda = 1.5045 \text{ \AA}$). The surface morphology of the as-prepared samples was inspected using JEOL JSM-7500F SEM. TEM images were recorded on JEM-2010 transmission electron microscope under a working voltage of 200 kV equipped with EDX spectrometer. XPS experiments were measured using an ESCALAB 250 Analytical XPL Spectrometer with a monochromatic Al K α source. All the binding energies were referenced to the C1s peak at 284.8 eV of the surface adventitious carbon. The Electrochemical measurements were performed on a model CHI630D electrochemical analyzer (ChenHua Instruments Co. Ltd., Shanghai, China). All experiments were conducted using a three-electrode electrochemical cell with a FTO based working electrode, an Ag/AgCl reference electrode, and a platinum wire counter electrode. EIS measurements were performed on a model CHI660D electrochemical analyzer (ChenHua Instruments Co. Ltd., Shanghai, China) in a PBS solution containing 5.0 mM K₃Fe(CN)₆ solution, and the bias potential was 0.25 V by applying an AC voltage with 5 mV amplitude in a frequency range from 0.01 Hz to 100 kHz under open circuit potential conditions and plotted in the form of complex plane diagrams (Nyquist plots).

- Zhai, D. Y. *et al.* Highly sensitive glucose sensor based on Pt nanoparticle/polyaniline hydrogel heterostructures. *ACS Nano* **4**, 3540–3546 (2013).
- Kros, A. *et al.* Poly(3, 4-ethylenedioxythiophene)-Based Glucose Biosensors. *Adv. Mater.* **13**, 1555–1557 (2001).
- Shafer-Peltier, K. E. *et al.* Toward a glucose biosensor based on surface-enhanced raman scattering. *J. Am. Chem. Soc.* **125**, 588–593 (2003).
- Niu, X. H. *et al.* Electrochemical sensing interfaces with tunable porosity for nonenzymatic glucose detection: A Cu foam case. *Biosens. Bioelectron.* **51**, 22–28 (2014).
- Niu, X. H. *et al.* Highly sensitive and selective nonenzymatic detection of glucose using three-dimensional porous nickel nanostructures. *Anal. Chem.* **85**, 3561–3569 (2013).
- Jiang, L. C. & Zhang, W. D. A highly sensitive nonenzymatic glucose sensor based on CuO nanoparticles-modified carbon nanotube electrode. *Biosens. Bioelectron.* **25**, 1402–1407 (2010).
- Sumanta, K. M. & Rao, G. R. Archetypal sandwich-structured CuO for high performance non-enzymatic sensing of glucose. *Nanoscale* **5**, 2089–2099 (2013).
- Kajal, J. *et al.* CuO thin film based uric acid biosensor with enhanced response characteristics. *Biosens. Bioelectron.* **38**, 11–18 (2012).
- Dung, N. Q., Patil, D., Jung, H. & Kim, D. A high-performance nonenzymatic glucose sensor made of CuO–SWCNT nanocomposites. *Biosens. Bioelectron.* **42**, 280–286 (2013).
- Chen, X., Zhang, N. Q. & Sun, K. N. Facile fabrication of CuO 1D pine-needle-like arrays for super-rate lithium Storage. *J. Mater. Chem.* **22**, 15080 (2012).
- Zhang, X. J. *et al.* Different CuO nanostructures: synthesis, characterization, and applications for glucose sensors. *J. Phys. Chem. C* **112**, 16845–16849 (2008).
- Ding, R. M. *et al.* Mixed Ni–Cu-oxide nanowire array on conductive substrate and its application as enzyme-free glucose sensor. *Anal. Methods* **4**, 4003 (2012).
- Chen, J. S. *et al.* Electrospun three-dimensional porous CuO/TiO₂ hierarchical nanocomposites electrode for nonenzymatic glucose biosensing. *Electrochem. Chem.* **20**, 75–78 (2012).
- Wei, Y. Y. *et al.* ZnO nanorods/Au hybrid nanocomposites for glucose biosensor. *Biosens. Bioelectron.* **26**, 275–278 (2010).
- Luo, J. T. *et al.* A new type of glucose biosensor based on surface acoustic wave resonator using Mn-doped ZnO multilayer structure. *Biosens. Bioelectron.* **49**, 512–518 (2013).
- Zhao, Z. W. *et al.* A novel amperometric biosensor based on ZnO: Co nanoclusters for biosensing glucose. *Biosens. Bioelectron.* **23**, 135–139 (2007).
- Muhammad, H. A. *et al.* Functionalised ZnO-nanorod-based selective electrochemical sensor for intracellular glucose. *Biosens. Bioelectron.* **25**, 2205–2211 (2010).
- Sathishkumar, P. *et al.* Synthesis of CuO–ZnO nanophotocatalyst for visible light assisted degradation of a textile dye in aqueous solution. *Chem. Eng. J.* **171**, 136–140 (2011).
- Niyanta, D. *et al.* Role of various interfaces of CuO/ZnO random nanowire networks in H₂S sensing: An impedance and Kelvin probe analysis. *Sensors and Actuators B* **202**, 1270–1280 (2014).
- Huang, J. R. *et al.* Preparation of porous flower-like CuO/ZnO nanostructures and analysis of their gas-sensing property. *J. Alloy Compd.* **575**, 115–122 (2013).
- Xu, Z. K. *et al.* CuO–ZnO micro/nanoporous array-film-based chemosensors: new sensing properties to H₂S. *Chem. Eur. J.* **20**, 6040–6046 (2014).
- Xia, H. *et al.* Solution-free, in situ preparation of nano/micro CuO/ZnO in dielectric barrier discharge for sensitive cataluminescence sensing of acetic acid. *Analyst* **138**, 3687–3691 (2013).
- Liu, J. P. *et al.* Hierarchical nanostructures of cupric oxide on a copper substrate: controllable morphology and wettability. *J. Mater. Chem.* **16**, 4427–4434 (2006).
- Sun, Z. Q. *et al.* Morphology-controllable 1D–3D nanostructured TiO₂ bilayer photoanodes for dye-sensitized solar cells. *Chem. Commun.* **49**, 966–968 (2013).
- Chuang, Y. C. *et al.* Crystal engineering from a 1D chain to a 3D coordination polymer accompanied by a dramatic change in magnetic properties. *Chem. Commun.* **48**, 10769–10771 (2012).
- Li, Z. Q., Ding, Y., Xiong, Y. J., Yang, Q. & Xie, Y. One-step solution-based catalytic route to fabricate novel a-MnO₂ hierarchical structures on a large scale. *Chem. Commun.* 918–920; DOI: 10.1039/B414204 (2005).
- Liu, Z. Y. *et al.* Hierarchical CuO/ZnO membranes for environmental applications under the irradiation of visible light. *Int. J. Photoenergy* **11**, 804840 (2012).
- Sahay, R. *et al.* Synthesis and characterization of CuO nanofibers, and investigation for its suitability as blocking layer in ZnO NPs based dye sensitized solar cell and as photocatalyst in organic dye degradation. *J. Solid State Chem.* **186**, 261–267 (2012).
- Tetsuro, S. *et al.* Alkaline vapor oxidation synthesis and electrocatalytic activity toward glucose oxidation of CuO/ZnO composite nanoarrays. *Appl. Surf. Sci.* **277**, 192–200 (2013).
- Yoon, M. *et al.* Composition-tuned ZnO–CdSe core-shell nanowire arrays. *ACS nano* **4**, 3789–3800 (2010).
- Xu, L. *et al.* NiO@ZnO heterostructured nanotubes: coelectrospinning fabrication, characterization, and highly enhanced gas sensing properties. *Inorg. Chem.* **51**, 7733–7740 (2012).
- Shin, S. *et al.* Novel Cu/CuO/ZnO hybrid hierarchical nanostructures for non-enzymatic glucose sensor application. *J. Electroanal. Chem.* **717–718**, 90–95 (2014).
- Ye, D. X. *et al.* A novel nonenzymatic sensor based on CuO nanoneedle/graphene/carbon nanofiber modified electrode for probing glucose in saliva. *Talanta* **116**, 223–230 (2013).
- Lin, Z. Y. *et al.* CuO–Ag₂O nanoparticles grown on a AgCuZn alloy substrate in situ for use as a highly sensitive non-enzymatic glucose sensor. *Anal. Methods* **6**, 2215–2220 (2014).
- Meng, F. H. *et al.* Nonenzymatic biosensor based on Cu₂O nanoparticles deposited on polypyrrole nanowires for improving detection range. *Biosens. Bioelectron.* **42**, 141–147 (2013).
- Zhuang, Z. J. *et al.* An improved sensitivity non-enzymatic glucose sensor based on a CuO nanowire modified Cu electrode. *Analyst* **133**, 126–132 (2008).
- Liu, G. Y. *et al.* Improvement of sensitive CuO NFs–ITO nonenzymatic glucose sensor based on in situ electrospun fiber. *Talanta* **101**, 24–31 (2012).
- Ahmad, R. *et al.* Wide linear-range detecting nonenzymatic glucose biosensor based on CuO nanoparticles inkjet-printed on electrodes. *Anal. Chem.* **85**, 10448–10454 (2013).
- Li, Y. *et al.* Facile synthesis of leaf-like CuO nanoparticles and their application on glucose biosensor. *Electroanalysis* **2**, 497–502 (2011).
- Tian, L. L. *et al.* Fabrication of CuO nanosheets modified Cu electrode and its excellent electrocatalytic performance towards glucose. *Appl. Surf. Sci.* **283**, 947–953 (2013).
- Cao, F. *et al.* Highly sensitive nonenzymatic glucose sensor based on electrospun copper oxide-doped nickel oxide composite microfibers. *Talanta* **86**, 214–220 (2011).
- Hsu, Y. W. *et al.* Synthesis of CuO/graphene nanocomposites for nonenzymatic electrochemical glucose biosensor applications. *Electrochimica Acta* **82**, 152–157 (2012).
- Eliot, R. *et al.* CuO nanospheres based nonenzymatic glucose sensor. *Electroanalysis* **20**, 2482–2486 (2008).
- Medina-Castillo, A. L. *et al.* One-step fabrication of multifunctional core-shell fibres by co-electrospinning. *Adv. Funct. Mater.* **21**, 3488–3495 (2011).

Acknowledgments

This work was supported by the National Natural Science Foundation of China (Grant no. 61204015, 81301289, and 61177042), Program for Chang Jiang Scholars and Innovative Research Team in University (No. IRT13018). The China Postdoctoral Science Foundation Funded Project (2012M511337 and 2013T60327), and the Jilin Province Natural Science Foundation of China (No. 20140101171J). Project 2014094 Supported by Graduate Innovation Fund of Jilin University.



Author contributions

C.Y.Z. conducted the most of investigation for the samples and wrote the main paper. L.X. supervised the project, had given valuable advices on the proceeding of this work, and revised the manuscript. J.S. D.L.L. and H.W.S. had provided precious suggestions on the selection of test and analysis of experimental data about electrospinning. R.Q.X. and S.X. supported the characterization of the samples. All authors discussed the results and commented on the manuscript at all stages.

Additional information

Supplementary information accompanies this paper at <http://www.nature.com/scientificreports>

Competing financial interests: The authors declare no competing financial interests.

How to cite this article: Zhou, C. *et al.* Ultrasensitive non-enzymatic glucose sensor based on three-dimensional network of ZnO-CuO hierarchical nanocomposites by electrospinning. *Sci. Rep.* **4**, 7382; DOI:10.1038/srep07382 (2014).



This work is licensed under a Creative Commons Attribution-NonCommercial-NoDerivs 4.0 International License. The images or other third party material in this article are included in the article's Creative Commons license, unless indicated otherwise in the credit line; if the material is not included under the Creative Commons license, users will need to obtain permission from the license holder in order to reproduce the material. To view a copy of this license, visit <http://creativecommons.org/licenses/by-nc-nd/4.0/>